Persistent fontanelles in Chihuahuas and inter- and intra-rater reliability of fontanelle area measurement in computed tomography images

Anna-Mariam Kiviranta (anna-mariam.kiviranta@helsinki.fi)
Helsingin Yliopisto https://orcid.org/0000-0002-9542-7247
Clare Rusbridge
University of Surrey
Anu K. Lappalainen
Helsingin Yliopisto
Jouni J.T. Junnila
4Pharma Ltd.
Tarja S. Jokinen
Helsingin Yliopisto

Research article

Keywords: brachycephaly, Chihuahua, craniosynostosis, fontanelle, ossification, syringomyelia

Posted Date: January 29th, 2020

DOI: https://doi.org/10.21203/rs.2.22165/v1

Version of Record: A version of this preprint was published on May 24th, 2021. See the published version at https://doi.org/10.1111/jvim.16151.

Abstract

Background: The Chihuahua dog breed is known for frequent occurrence of a bregmatic fontanelle on the dorsal skull. A common conception is that this skull defect is clinically irrelevant in Chihuahuas. No studies, however, describe the prevalence of this malformation, whether it is accompanied by fontanelles at other locations on the skull or how to assess the severity of these lesions. Our primary aim was, by using computed tomography imaging, to describe the presence, number, and location of persistent fontanelles (PF) at cranial sutures on dorsal, lateral and caudal cranial surfaces in Chihuahuas. The secondary aim was to develop a method to measure the fontanelle area in computed tomography images by using the closed polygon tool of Osirix Medical Imaging Software.

Results: Of the 50 dogs evaluated, 46 (92%) had either one or several PFs. The mean ± SD number of affected cranial sutures per dog was 2.4 ± 2.3 (range 0-10), and mean ± SD number of PFs was 2.8 ± 3.0 (range 0-13). Of the 46 dogs with affected sutures, 7 (15%) had no PF at a location typical for a bregmatic fontanelle. The inter-rater reliability of the fontanelle area measurement was almost “perfect”, and intra-rater reliability reached “excellent” agreement.

Conclusions: PFs are almost ubiquitous in the examined group of Chihuahuas. They are located at dorsal, lateral, and caudal surfaces of the cranium, and hence are not all recognized reliably by palpation in adult dogs. Though the pathogenesis of the PFs described here is unknown, bone-deficient lesions may occur due to congenital defects in cranial bone ossification, delayed closure of cranial sutures, or bone resorption, as is observable in children with craniosynostosis (premature cranial suture closure). Because the imaging findings described in the Chihuahuas of this study are similar to findings among children with craniosynostosis/premature cranial base synchondrosis closure, this growth disorder may be a predisposing factor for the PFs described here. Further studies are necessary to evaluate the pathogenesis and clinical relevance of these lesions. Due to high inter- and intra-rater reliability of the method of fontanelle area measurement it may be useful in future studies.

Background

The Chihuahua is a dog breed known for its very small size, round head, and frequent occurrence of a bregmatic fontanelle (or molera) on the top of the skull, between the paired frontal and parietal bones. It is a common conception that the bregmatic fontanelle is clinically irrelevant in small-breed dogs, especially in Chihuahuas [1]. No studies, however, describe the prevalence of this malformation or state whether it is accompanied by fontanelles at other locations on the skull.

The skull consists of the viscerocranium forming the skeleton of the face and the neurocranium forming the cranial base and the cranial vault [2]. The neurocranium develops from mesodermal and neural crest cells during embryonic development [3]. The skull base (occipital, sphenoid, and ethmoid bones) develops through endochondral ossification, whereas the cranial roof (frontal, parietal, squamous part of the temporal bone, and interparietal part of the occipital bone) develops through membranous ossification [2, 4–6].

Fontanelles are fibrous, membrane-covered gaps that lie between the cranial bones formed by intramembranous ossification and at the intersection of the cranial sutures. The cranial sutures are the junctions between membranous bones, and between membranous and endochondral bones. They are the major sites of bone expansion—during post-natal cranial growth—of the cranial vault that will accommodate the enlarging brain. This expansion occurs in response to signals from the expanding neurocranium. By contrast, the endochondral bones, (i.e. cranial base bones), are connected by cartilaginous synchondroses and expand through chondrocyte hypertrophy [7].

At maturation, which disables further growth of the cranium, the cranial sutures close. Information concerning canine cranial suture closure times is scarce, but one suggestion is that the interparietal, i.e. sagittal, suture closes at the age of 2 to 3 years and the interfrontal, i.e. metopic suture at the age of 3 to 4 years [8]. In humans, cranial sutures close during the third decade of life [7].

Children are born with six fontanelles: two along the midline, the anterior (also called as the bregmatic fontanelle) and the posterior fontanelle, and two on each side of the skull, the left and right sphenoid, and left and right mastoid fontanelles [9]. The largest fontanelle in children, the anterior fontanelle, is located at the junction of the two frontal and parietal bones and closes between 3 to 27 months, with the median age of closure ranging from 9 to 14 months [10, 11]. The posterior fontanelle is located between the occipital and two parietal bones, is open in only 1.5% of newborn children, and closes in those children by 2 months of age [12]. Furthermore, the paired sphenoid fontanelles occur at the intersection of the frontal, parietal, sphenoid, and temporal bones and close at around 3 months of age. Caudal to the sphenoid fontanelles, and between the parietal, temporal and occipital bones, are the mastoid fontanelles that close during the second year of life [13].

In dogs, few studies describe the fontanelle-closure times, and those that do, only describe the bregmatic and occipital fontanelle closure times: Bregmatic fontanelle closure is assumed to occur at birth or within a month afterwards [5, 14]. The fontanelle resembling the posterior fontanelle in children, here we call the occipital fontanelle, closes at around 45 days of gestation when the unpaired interparietal bone fuses

with the parietal and supraoccipital bones. In some dogs, the interparietal bone does not fuse with the supraoccipital bone, and remains as a separate bone [5].

In Chihuahua breed standards of different kennel clubs the occurrence of a molera, a persistent fontanel (PF) at the intersection of the paired frontal and parietal bones, varies from being an accepted trait to being a disqualifying fault [15–18]. The existence of this PF is commonly tested by palpating the head, which only enables the recognition of PF in areas of the skull lacking a thick muscle layer such as the mid-dorsal region (the location of the bregmatic fontanelle). Cranial computed tomography (CT) imaging provides more complete assessment permitting determination of how common PFs are in Chihuahuas and also if these skull defects occur on cranial surfaces not detected by palpation. Developing an objective method to evaluate the severity of these lesions would in the future allow assessment of the clinical relevance and pathogenesis of these findings in Chihuahuas. In children, sutural diastasis (delayed closure of a cranial suture) and disorders of cranial ossification are associated with developmental disorders of cranial growth due to premature cranial suture closure [19]. Reliable diagnostic methods would allow comparison between the pathogenesis of PFs in Chihuahuas and bone deficient skull lesions in children.

The primary objective of our prospective study was to describe the presence, number, and location of PFs in Chihuahuas. The secondary objective was to evaluate the inter- and intra-rater reliability of the fontanelle area measurement method in CT images. Our primary hypothesis was that PFs are common in Chihuahuas and occur not only at the intersection of the frontoparietal, sagittal, and interfrontal sutures—hence at the location of the bregmatic fontanelle—but at other locations, as well. Our secondary hypothesis was that the fontanelle-area measurement method is repeatable both by different evaluators and between separate measurement times (inter- and intra-rater reliabilities).

Results

The study group of 50 Chihuahuas comprised 26 (52%) smooth-haired, 23 (46%) long-haired Chihuahuas, and 1 (2%) Chihuahua mix. These comprised 27 (54%) females and 23 (46%) males (including one castrated male). The mean ± SD age of these 50 dogs was 58 ± 28 months (range 7-139 months), and their mean ± SD weight was 2.8 ± 0.6 kg (range, 1.4–4.3 kg). Of the 50 included dogs 21 were not clinically affected and 29 had clinical signs related to Chiari-like malformation or syringomyelia (CM/SM). Of those 29 clinically affected dogs, 7 dogs had concurrent diseases possibly causing similar clinical signs than CM/SM.

Presence, number, and location of persistent fontanelles

Of the 50 dogs evaluated, 46 (92%) had either one or several PF. The mean ± SD number of affected sutures per dog was 2.4 ± 2.3 (range 0-10), and mean ± SD number of PFs was 2.8 ± 3.0 (range 0-13). Due to one dog that had missing CT images of the very rostral skull, the cohort for evaluation of distribution of affected sutures and PFs comprised 49 dogs. A total of 34 dogs (69%) had 1 to 3 affected sutures, 7 dogs (14%) had 4 to 6 such sutures, and 4 dogs (8%) had 7 to 10. Similarly, grouping dogs by their number of PFs showed that of 49 dogs, 32 (65%) had 1 to 3 PFs, 7 (14%) had 4 to 6 PFs, and 6 (12%) had 7 to 13. (Tables 1 and 2).

A total of 118 affected sutures occurred in these 49 dogs: 57 (48%) occurred dorsally, 44 (37%) caudally, and 17 (14%) laterally (7 on the left side, 10 on the right side). Furthermore, of the total 138 PFs, 72 (52%) appeared dorsally, 49 (36%) caudally, and 17 (12%) laterally (7 on the left side, 10 on the right side) (Table 3).

Of the 46 dogs with affected sutures, 7 (15%) had no PF at a location typical of a bregmatic fontanelle. Of those dogs, each dog had 1 to 7 affected sutures on either dorsal, lateral, or caudal surfaces of the cranium. Furthermore, 44 (32%) of the 138 fontanelles occurred in other locations than those in children (the anterior, posterior, sphenoid, or mastoid fontanelles).

The number of the PFs varied from single (Figure 1) to multiple lesions (Figure 2) at one suture, and the shape from sharply edged (Figure 3) to lesions with non-distinct margins (Figure 4). Occasionally, the lesions appeared to be connected to radiolucent lines resembling venous structures (Figure 5).

Inter- and intra-rater reliability of persistent fontanelle area measurement in computed tomography images

The inter-rater repeatability of the total fontanelle area measurements between the assessors was 99.8%. When assessing consistency between the two assessments, Krippendorff's alpha for the total fontanelle area was 0.999 (95% CIs 0.997-1.000) (Table 4).

The intra-rater repeatability of the total fontanelle area measurements were 99.6 % for one and 99.8% for the other assessor. Furthermore, the intra-class correlation coefficient (ICC) for reliability within assessor of the total fontanelle area ranged from 0.997 to 0.999, (95% confidence intervals (CI) 0.994-0.999) (Table 5).

Discussion

Our study shows that according to our primary hypothesis cranial bone lesions, called here PFs, are a common finding in adult Chihuahuas. In addition to their well-known location on the dorsal surface of the cranium (i.e. the bregmatic fontanelle at the intersection of the frontoparietal, sagittal, and interfrontal sutures), PFs are common on other sutures located on the lateral and caudal surfaces of the skull as well. Similarly, according to the secondary hypothesis, the method used in the current study for PF area measurement was reliable as it showed almost “perfect” inter-rater and “excellent” intra-rater reliability and can thus be utilized in further studies.

Persistent fontanelles

The Chihuahuas of this study almost all had either one or several PFs. The PF occurred on all cranial surfaces, with approximately half of all PFs occurring on the dorsal surface and slightly over one-third occurring on the caudal surface of the cranium (Fig. 6). Clinically this is significant as, in dogs, other locations than the site of the bregmatic fontanelle (mid-sagittal, dorsal surface of the cranium) are covered with muscles thick enough to prevent reliable recognition by palpation.

The frontoparietal suture, the location of the bregmatic fontanelle, was the suture most commonly affected. The bregmatic fontanelle, however, was not always present although the dog had other affected sutures. This prevents the use of the bregmatic fontanelle as a marker of these bony lesions elsewhere on the cranial surface. Furthermore, because magnetic resonance imaging is less sensitive than CT in detecting open sutures, the common use of magnetic resonance images to rule out structural brain diseases could predispose small PFs to being overlooked [20].

Only the bregmatic and caudally located fontanelle, resembling the human posterior fontanelle, and here called the occipital fontanelle, are described in dogs, with the literature lacking the descriptions of the sphenoid and mastoid fontanelles. Furthermore, although the lesions are here called PFs, one-third of the PFs occurred at locations other than the locations similar to those of the fontanelles described in children. Hence, additional etiologies may exist than just delayed fontanelle closure.

Areas deficient in bone can occur, for example due to disorders of ossification of the developing bone, atrophy of mature bone, or sutural diastasis (delayed closure). Based on the current study design, and with all but two Chihuahuas of this study having been aged over 12 months, it is not possible to evaluate whether the PFs described here are congenital defects of bone formation or acquired bone remodeling or bone atrophy. It is generally thought that the bregmatic fontanelle is a common finding in immature Chihuahuas, one suggestive of, but not conclusively considered to be a congenital lesion. As the PFs on the remainder of the skull surface are not recognizable by palpation, the nature of those lesions remains particularly inconclusive. Both forms of acquired bone defects, i.e., bone remodeling and bone atrophy, occur in dogs: In cavalier King Charles spaniels, similarly affected with CM as are Chihuahuas, foramen magnum height increases over time, suggesting active supraoccipital bone remodeling due to cerebellar pulsation [21–23]. Furthermore, suggestive of bone atrophy, skull bone defects can occur as a result of multiple choroid plexus carcinomas leading to non-communicating hydrocephalus and increased intracranial pressure [24].

To better evaluate all possible causes behind the bone-deficient lesions here described, understanding skull development, ossification, and cranial growth is pivotal: intramembranous ossification of the bones of the cranial vault is initiated by condensation of mesenchymal cells between the dermal epithelium and the forming meninges [2]. The mesenchymal cells differentiate to become first osteoblasts and later osteocytes that produce bone-forming matrix. In the endochondral ossification, the mesenchymal cells differentiate into hypertrophic chondrocytes that form an avascular anlagen, a cartilaginous template that is later replaced by bone [25].

Cranial growth occurs at the synchondroses and at the cranial sutures: The synchondroses allow rostrocaudal expansion of the cranial base, and the cranial vault growth occurs perpendicular to the cranial sutures. The pace of the mesenchymal cells differentiating into osteoblasts, regulated by the growing brain via dura mater, affects bone growth at cranial suture growth sites. In addition to sutural bone growth, constant modeling and remodeling of both at the inner- and outer surfaces of the bone occurs to fit the surrounding tissues, such as the contours of the brain [2, 25]. Cranial sutural growth normally continues until the brain has matured, and the cranial base synchondroses continue to lengthen. To enable membranous bone growth, the cranial sutures need to remain in an un-ossified state [7]. Abnormal osteoblast apoptosis at the cranial sutures causes premature cranial suture closure, craniosynostosis [26]. This prevents future bone formation, and hence expansion of the neurocranium at the site of the closed cranial suture, and leads to abnormal compensatory cranial growth [7].

In children, premature cranial suture closure, craniosynostosis, is a rare growth disorder, occurring in approximately 3 to 7 of every 10 000 live births and disabling normal expansion of the skull [27–28]. It prevents normal bone growth perpendicular to the affected suture and results in a characteristic head-shape typical of that type of craniosynostosis. For example, a bilateral coronal suture synostosis (between the frontal and parietal bones) causes shortening of the skull and results in brachycephaly [29]. As craniosynostosis causes certain sutures to close prematurely, as compensation, it may delay or prevent others from closing (sutural diastasis). As a result, children with craniosynostosis are more likely to have sutural diastasis [19]. Additionally, in children, craniosynostosis can occur simultaneously with premature cranial base synchondrosis closure [30].

In brachycephalic dogs, and especially in cavalier King Charles spaniels, the cranial base spheno-occipital synchondrosis closes prematurely, restricting rostocaudal skull expansion [31]. As a sign of compensatory cranial growth due to premature cranial suture and synchondrosis closure in brachycephalic dogs, a higher proportion of closed or closing rostral cranial sutures or cranial base synchondroses was associated with dorsal deviation of the prebasial angle, also called airorynchy [32]. Furthermore, in Chihuahuas, a short skull base at the caudal cranial fossa causes overcrowding of the craniocervical junction. Such overcrowding predisposes to both SM and CM/SM-related clinical signs [23, 33]. Furthermore, in cavalier King Charles spaniels, brachycephaly, i.e. a short skull base with compensatory doming of the skull, is associated with CM-associated pain [34].

Differences in synchondrosis and in cranial suture-closure times, described in early morphometric studies, could explain the large variance in skull dimensions of different dog breeds [35]. To support that theory, a recent study described the premature closure of the sagittal suture as possibly explaining the typically high head-shape of the boxers [20]. Furthermore, a later study, evaluating head-shape inheritance, showed that, for facial-length variation between dog breeds, a SMOC2 locus explained 36%. It suggests that the cranial suture closure times appear genetically regulated [36].

Many of the PFs in the Chihuahuas of this study occurred at other than the expected fontanelle locations. In children, non-fontanelle cranial bone defects occur, ones such as lacunar skull and diffuse copper-beaten appearance: lacunar skull, also called “Lückenshädel skull” (German for holes in the skull), is a developmental, congenital defect of bone ossification, whereas the copper-beaten appearance is an acquired remodeling of bone [37]. Both of these lesions affect the inner table of the cranial vault, causing either thinning or loss of bone, with the copper-beaten pattern appearing with indistinct margins, varied depth, and following the gyral margins. On the other hand, lacunar skull defects have sharply demarcated margins and are separated by branches of bone [19, 38–40]. A lacunar skull, when occurring with full-thickness defects, is also called craniofenestra [41]. Both the copper-beaten appearance and lacunar skull are associated with craniosynostosis, but can also occur as incidental findings [19].

In our Chihuahuas, the shape of PFs varied; some comprised sharply demarcated, full-thickness lesions showing similarities with lacunar skull defects (including craniofenestra). On the other hand, sometimes the PFs had indistinct margins and were surrounded by areas of thin bone, suggesting a more active bone remodeling, though lacking the gyral pattern and diffuse distribution of the copper-beaten appearance. Copper-beaten appearance is previously described in a Griffon Bruxellois with clinically relevant CM and SM [42].

Some of the PFs appeared to occur in close proximity to radiolucent areas resembling venous structures. This could be a consequence of active bone remodeling due to increased venous pressure. In cavalier King Charles spaniels, cranial-base shortening due to premature synchondrosis closure is suspected to cause venous outflow obstruction resulting from narrowed jugular foramina [43]. Supporting a theory of decreased venous outflow through the jugular foramina, another study described decreased volumes of caudal cranial fossa venous sinuses in syringomyelia-affected cavalier King Charles spaniels [44]. Jugular foramen obstruction occurs also in achondroplastic children with premature synchondrosis closure. In those children, a shortened skull base leads to jugular foramen stenosis and, due to increased venous pressure, may cause communicating hydrocephalus [45]. Furthermore, in children, craniosynostosis may occur alongside enlarged emissary veins [46].

Inter-rater and intra-rater reliabilities of fontanelle area measurement

Repeatability of total, dorsal, left and right lateral, and caudal fontanelle-area measurements between the assessors, the inter-rater reliability, was almost perfect when assessing both the percentage agreement and Krippendorff’s alpha. Similarly, repeatability of the total, dorsal, left and right lateral, and caudal fontanelle area within the same assessor, the intra-rater reliability, reached excellent reliability when assessing both percentage agreement and ICC. Hence, the excellent inter- and intra-rater reliabilities reported in this study suggest that the fontanelle area measurement is method is suitable for further use.

Our excellent results can be thus explained: we obtained all CT images with the same scanner, we set clear guidelines for the measurement method while evaluating the pilot dogs (not included in the final analysis), and each evaluator used the same computer screen while analyzing all the CT images (intra-rater reliability). Furthermore, though neither of the evaluators had previous experience with the current

method, both were experienced in analyzing cranial CT images. On the other hand, differences in index-line positioning and placement of the area borders of the closed polygon tool explain why the evaluators did not reach a perfect consensus.

Though descriptions of similar fontanelle area measurement are lacking, earlier studies describe measurement of the canine cranial cavity, caudal cranial fossa, or foramen magnum areas using either CT or magnetic resonance imaging [47–50]. Furthermore, several studies describe volumetric measurements of the canine cranial cavity [44, 51–54]. None of these studies describes intra- or inter-rater reliabilities, possibly due to the laboriousness of the area- and volume-measurement methods. In children, one study describes its anterior fontanelle area measurement in CT images: calculation of the surface area involved multiplying the width of the fontanelle by its anterioposterior length, and dividing it by two [55]. Due to the irregular shape of the fontanelles in dogs, we did not adopt that same formula.

Limitations of this study were related to its image analysis and cohort collection: Evaluation of the presence of PFs was occasionally difficult due to very thin bone, and the low spatial resolution provided by the imaging equipment (2-slice CT), making it sometimes difficult to differentiate between thinning of bone from a true, full-thickness lesion. Furthermore, as the cranial sutures were difficult to define, it was occasionally challenging to determine the exact location of the lesion. However, consensus between our evaluators improved the accuracy of the classification of the lesions, both as to their presence and location. As the aim of the study was to describe the occurrence of these bony lesions, we did not attempt to group them based on their possible etiology (such as congenital defect of ossification or as active bone remodeling/atrophy). Furthermore, as most of the dogs were alive at the end of the study, they did not undergo an autopsy to compare the CT-area measurement findings with the actual PF areas in cadaveric skulls. Finally, the majority of the Chihuahuas were from the same country, making multicenter studies evaluating international cohorts essential.

Conclusions

In conclusion, the lesions described, here called PFs, are, in this group of Chihuahuas, very common and almost ubiquitous. The number of PFs varied, per dog, from single to multiple. They were located on dorsal, lateral, and caudal surfaces of the cranium, and hence were not all reliably recognizable by palpation. The PF area measurement method described here appears reliable both between different assessors and at different measurement times. The PFs described in this group of Chihuahuas show some similarities with the imaging findings of bone-deficient lesions in craniosynostotic children. Though additional studies are necessary to evaluate the pathogenesis of the PFs in Chihuahuas, notable similarities with the imaging findings suggest that premature synchondrosis closure or craniosynostosis or both may prove to be predisposing factors also in Chihuahuas. Understanding the mechanisms responsible for the PFs in Chihuahuas may therefore in the future provide additional information for the mechanisms of craniosynostosis in children.

Materials And Methods

Case selection and assessment of clinical signs

Our prospective data included 50 Chihuahuas, members of the same cohort (comprising 53 Chihuahuas) participating in another, concurrent study published earlier: The study included client-owned Chihuahuas with or without CM/SM-related clinical signs. The dogs were recruited from the case-load of the Veterinary Teaching Hospital of the University of Helsinki between 2012–2015. Imaging of the clinically affected dogs was a diagnostic procedure and the non-affected dogs were imaged for breeding selection to detect CM, SM, and craniocervical junction overcrowding [23]. Non-affected dogs had to be at least three years old, but no age limit was set for clinically affected dogs. All the dogs with a prior history of a central nervous system disease (other than CM, SM or craniocervical junction overcrowding) or a severe orthopedic problem were excluded. The study was approved by the Finnish National Animal Experiment Board, participation was voluntary, and all dog owners provided a written consent. The current study included all the dogs from the earlier study that underwent CT to evaluate the craniocervical junction. All the procedures were undertaken during one visit at the Veterinary Teaching Hospital.

Two of the clinically affected dogs with previous history of epileptic seizures were euthanized due to status epilepticus during anesthesia recovery and recurrent epileptic seizures for > 48 hours. Epileptic seizures recurred though the dogs were medicated first with loading doses of phenobarbital (24 mg/kg iv), levetiracetam (60 mg/kg iv), and potassium bromide (400–600 mg/kg p.r.), and then with maintenance doses of the same medications (phenobarbital 3 mg/kg every 12 hours i.v., levetiracetam 20 mg/kg every 8 hours i.v., potassium bromide 10 mg/kg every 12 hours p.r.) and continuous rate infusions of either propofol or dexmedetomidine and midazolam. Both dogs were euthanized due to humane reasons and by owner request. One of the dogs was euthanized at The Veterinary Teaching Hospital: after sedation with intravenous administration of dexmedetomidin and butorphanol, boluses of intravenous propofol and pentobarbitone were administered until cardiac arrest occurred. The other dog was euthanized at their local veterinarian after being discharged at owner's request from the intensive care unit of The Veterinary Teaching Hospital. All the other dogs remained alive at the end of the study. As the dogs were client-owned, none of the dogs were released and they returned to live in home-environment with their owners. The clinically affected dogs continued to have control

visits at The Veterinary Teaching Hospital, at the referring/local veterinarian or were lost from follow-up. No further visits occurred in the clinically non-affected dogs, but the owners could contact the first author in case questions emerged.

Diagnostic imaging procedures

All dogs underwent CT under general anesthesia. An anesthesiologist planned the anesthesia individually for each patient. During anesthesia, heart and respiratory rate, blood pressure, and end-tidal carbon dioxide partial pressure were monitored. To obtain head and cervical spine (to the level of the caudal C3 vertebra) CT images, we used a helical dual-slice CT scanner (Somatom Emotion Duo, Siemens AG, Forcheim, Germany), with a bone algorithm and a slice thickness of 1.0 mm (feed/rotation 2 mm, reconstruction increment 0.5 mm). The dogs were positioned so that the base of the skull was aligned perpendicular to the ventral vertebral canal in the cranial cervical spine. Our previous study provides full CT imaging details [23].

Image analysis

OsiriX Medical Imaging Software (Pixmeo SARL, Bernex, Switzerland) served for analysis of the CT images of all included dogs for presence, number, and location of the PFs, and the fontanelle areas at dorsal, lateral, and caudal cranial sutures. Additionally, the total fontanelle area was calculated using the closed polygon tool of the software.

Presence of persistent fontanelles

A persistent fontanelle was defined as full-thickness loss of bone at a cranial suture. Its presence was assessed at the cranial sutures, i.e. the junctions between the membrane-derived bones (nasal, lacrimal, frontal, parietal, interparietal, squamous part of the temporal) and between the membrane- and cartilage-derived bones (maxillary, palatine, sphenoid, temporal, occipital) which form the dorsal, lateral, and caudal surfaces of the braincase. The cranial base, formed of cartilage-derived bones connected with synchondroses, and naturally occurring with multiple foramina, was not evaluated (see Table 3, Figs. 7–9). To improve the method's reliability and to exclude non-fused, normal cranial sutures, the fontanelle area had to be large enough, by subjective assessment, to be measurable using the closed polygon tool. The smallest PFs measured were approximately 1 mm in diameter.

As the distinction between some dorsal and lateral bones was difficult, due to their small size and irregular shape, we made no attempt to distinguish between them, and the sutures were classified as one (Table 3, Fig. 7, No. 1; Fig. 8, No. 7). Furthermore, as a PF was occasionally located between the supraoccipital and interparietal bones, though not at a true suture, and as these two bones, in adult dogs, are suggested to be fused, the junction between them was considered an additional location (Table 3, Fig. 9, No. 16) [5]. Additionally, the intersections of the lateral sutures, ones resembling sphenoid (Table 3, Fig. 8, N:o 8) and mastoid fontanelles in children (Table 3, Fig. 9, No 12 and 13), were classified as additional locations [13].

Two board-certified neurologists (A-M.K. and T.S.J.) evaluated independently the anonymized CT images and were hence unaware of the dogs' clinical status. The evaluators first assessed each cranial suture in 3-dimensional skull models using volume-rendering technique images to record the presence and number of all possible PFs (Fig. 1), and then confirmed their findings in the multiplanar images (Figs. 10a-c). If after the individual assessment, the evaluators did not agree about the presence or number of PFs, or as to the sutures affected, the evaluators re-assessed the CT images together to reach a consensus. The evaluators agreed that all the assessed PFs were located at cranial sutures.

Total fontanelle area

After the consensus, the evaluators independently measured the area of each fontanelle from the anonymized CT-images using the closed polygon tool (Fig. 11). Because in dogs no studies describe the PF area measurement method, we first tested it by assessing CT images of 10 pilot dogs, ones not included in the study. The following guidelines were set: The fontanelle area measurement was carried out by means of multiplanar CT images (WL 500 HU, WW 3500 HU) with one of the two index lines positioned tangential to the outer skull surface, and in the mid-thickness of the bone surrounding it. Then, the other index line was positioned perpendicular to the previous index line and in the center of the PF (Figs. 10a-c). As the area of the PF was occasionally large and extended over convex surfaces, making it impossible to measure it reliably in one plane, we used a maximum-intensity–projection-technique image, with slice thickness of 14 to 16. This slice thickness was selected by visually optimizing the ability to measure also convex surfaces and without the area to be measured being affected. While measuring the pilot dogs' fontanelle areas, the evaluators had the possibility to discuss the measurement technique to optimize its reliability and reproducibility. When measuring the actual study dogs, the two evaluators measured the areas independently.

Statistical Analysis

First, to evaluate the reliability of the method for fontanelle area measurements, the inter-, and intra-rater reliabilities needed evaluation. We assessed the sum of dorsal, lateral, and caudal fontanelle areas both separately and as the total sum of all fontanelles. We evaluated the random variation caused by assessors (inter-rater reliability) in two different ways: First, we calculated a repeatability statistic between the assessors from a one-way analysis of variance model, where the effect of the dog served as the sole fixed effect, and the values were considered as a percentage of perfect agreement. In these models, the within-group variation describes the variation between the assessors.

Second, to determine inter-rater reliability estimate between the two assessors, we calculated Krippendorff's alpha with 95% confidence intervals (CI) to assess consistency between the two assessments of the fontanelle areas [56]. An alpha-value of 1 describes perfect agreement, a value of 0.8 describes similar interpretation, and a value ≥ 0.67 is interpreted as the lowest conceivable limit [57].

Next, we evaluated the intra-rater reliability: The two evaluators independently re-measured, after a few months' interval, a randomly selected 25 dogs among 50 dogs' fontanelle areas. Due to the laboriousness of the method 25/50 (50%) of the dogs' CT images were re-evaluated. The intra-rater reliability assessment took place by two different methods: first, we calculated a repeatability statistic similar to that for inter-rater reliability between the two repeats (total fontanelle area) by each evaluator. Second, to determine the intra-rater reliability estimate between the repeats, we calculated the ICC with 95% CIs to assess consistency between the repeats. An ICC of < 0.5 indicates poor reliability, 0.5–0.75 moderate reliability, 0.75–0.9 good reliability, and > 0.9 indicates excellent reliability [58]. All statistical analyses used the SAS® System for Windows, version 9.4 (SAS Institute Inc., Cary, NC, USA).

References

1. DeLahunta A, Glass E. Development of the Nervous System: Malformations. In Veterinary neuroanatomy and clinical neurology. St. Louis, Missouri: Saunders/Elsevier; 2009. p. 23-53.
2. Jin S, Sim K, Kim S. Development and Growth of the Normal Cranial Vault: An Embryologic Review. J Korean Neurosurg Soc 2016;59(3):192-196.
3. Couly GF, Coltey PM, Le Douarin NM. The triple origin of skull in higher vertebrates: a study in quail-chick chimeras. Development 1993;117(2):409-429.
4. Srivastava HC. Ossification of the membranous portion of the squamous part of the occipital bone in man. J Anat 1992;180:219-224.
5. Evans HE. The Fetus. In Miller's anatomy of the dog. 3rd ed. Philadelphia: Saunders; 1993. p. 48-97.
6. Knowler SP, Galea GL, Rusbridge C. Morphogenesis of Canine Chiari Malformation and Secondary Syringomyelia: Disorders of Cerebrospinal Fluid Circulation. Front Vet Sci 2018; 10.3389/fvets.2018.00171
7. Opperman LA. Cranial sutures as intramembranous bone growth sites. Dev Dyn 2000;219(4):472-485.
8. Thrall DE, Robertson ID. Atlas of Normal Radiographic Anatomy and Anatomic Variants in the Dog and Cat. St. Louis, Missourio: Elsevier/Saunders; 2011. p. 10
9. Kiesler J, Ricer R. The abnormal fontanel. Am Fam Physician 2003;67(12):2547-2552.
10. Duc G, Largo RH. Anterior fontanel: size and closure in term and preterm infants. Pediatrics 1986;78(5):904-908.
11. Boran P, Oğuz F, Furman A, Sakarya S. Evaluation of fontanel size variation and closure time in children followed up from birth to 24 months. J Neurosurg Pediatr 2018 09;22(3):323-329.
12. Esmaeili M, Esmaeili M, Ghane Sharbaf F, Bokharaie S. Fontanel Size from Birth to 24 Months of Age in Iranian Children. Iran J Child Neurol 2015;9(4):15-23.
13. Gray H, Standring S. editor. Standring S. In Gray's anatomy. 39. ed., Edinburgh: Elsevier, Churchill Livingstone; 2006. p. 457-458.
14. Hassan EA, Torad FA, El-Tookhy OS, Shamaa AA. Canine neonatal transcranial ultrasonography from birth until closure of bregmatic fontanelle. Top Companion Anim Med 2015;30(1):5-9.
15. American Kennel Club. http://images.akc.org/pdf/breeds/standards/Chihuahua.pdf. Accessed December 20 2019
16. Canadian Kennel Club. https://www.ckc.ca/CanadianKennelClub/media/Breed-Standards/Group%205/Chihuahua-Long-Short-Coat.pdf. Accessed December 20 2019
17. The Kennel Club. https://www.thekennelclub.org.uk/services/public/breed/standard.aspx?id=6150. Accessed December 20 2019
18. Federation Cynologicue Internationale http://www.fci.be/Nomenclature/Standards/218g09-en.pdf. Accessed December 20 2019
19. Tuite GF, Evanson J, Chong WK, Thompson DN, Harkness WF, Jones BM, Hayward RD. The beaten copper cranium: a correlation between intracranial pressure, cranial radiographs, and computed tomographic scans in children with craniosynostosis. Neurosurgery 1996;39(4):691-699.

20. Farke D, Guiller B, Oszewska A, Schmidt MJ. Sagittal craniosynostosis as underlying cause for unusual brain and skull morphology in boxers. In 32nd European College of Veterinary Neurology/European Society of Veterinary Neurology Annual Symposium; 13.-14.9.2019
21. Driver CJ, Watts V, Bunck AC, Van Ham LM, Volk HA. Assessment of cerebellar pulsation in dogs with and without Chiari-like malformation and syringomyelia using cardiac-gated cine magnetic resonance imaging. Vet J 2013;198(1):88-91.
22. Driver CJ, De Risio L, Hamilton S, Rusbridge C, Dennis R, McGonnell IM, et al. Changes over time in craniocerebral morphology and syringomyelia in cavalier King Charles spaniels with Chiari-like malformation. BMC Vet Res 2012;8:215.
23. Kiviranta A-M, Rusbridge C, Laitinen-Vapaavuori O, Hielm-Björkman A, Lappalainen AK, Knowler SP, et al. Syringomyelia and Craniocervical Junction Abnormalities in Chihuahuas. J Vet Intern Med 2017;31(6):1771-1781.
24. Hughes JR, Taylor-Brown FE, Greville-Heygate O, Constantino-Casas F, Williams DL, Genain M. Multimodality characteristics of multifocal choroid plexus carcinoma with bilateral calvarial defects in a dog. Vet Radiol Ultrasound 2019; https://doi.org/10.1111/vru.12732
25. Flaherty K, Singh N, Richtsmeier JT. Understanding craniosynostosis as a growth disorder. Wiley Interdiscip Rev Dev Biol 2016 07;5(4):429-459.
26. Rice DP, Kim HJ, Thesleff I. Apoptosis in murine calvarial bone and suture development. Eur J Oral Sci 1999;107(4):265-275.
27. Boulet SL, Rasmussen SA, Honein MA. A population-based study of craniosynostosis in metropolitan Atlanta, 1989-2003. Am J Med Genet A 2008;146A(8):984-991.
28. Cornelissen M, Ottelander Bd, Rizopoulos D, van der Hulst R, Mink van der Molen, Aebele, van der Horst C, Delye H, van Veelen ML, Bonsel G, Mathijssen I. Increase of prevalence of craniosynostosis. J Craniomaxillofac Surg 2016;44(9):1273-1279.
29. Governale LS. Craniosynostosis. Pediatr Neurol 2015;53(5):394-401.
30. Coll G, Sakka L, Botella C, Pham-Dang N, Collet C, Zerah M, Arnaud E, Di Rocco F. Pattern of Closure of Skull Base Synchondroses in Crouzon Syndrome. World Neurosurg 2018;109:e460-e467.
31. Schmidt MJ, Volk H, Klingler M, Failing K, Kramer M, Ondreka N. Comparison of closure times for cranial base synchondroses in mesaticephalic, brachycephalic, and Cavalier King Charles Spaniel dogs. Vet Radiol Ultrasound 2013;54(5):497-503.
32. Geiger M, Haussman S. Cranial Suture Closure in Domestic Dog Breeds and Its Relationships to Skull Morphology. Anat Rec (Hoboken) 2016;299(4):412-420.
33. Knowler SP, Kiviranta AM, McFadyen AK, Jokinen TS, La Ragione RM, Rusbridge C. Craniometric Analysis of the Hindbrain and Craniocervical Junction of Chihuahua, Affenpinscher and Cavalier King Charles Spaniel Dogs With and Without Syringomyelia Secondary to Chiari-Like Malformation. *PLoS One*. 2017;12(1):e0169898. Published 2017 Jan 25. doi:10.1371/journal.pone.0169898
34. Knowler SP, Cross C, Griffiths S, McFadyen AK, Jovanovik J, Tauro A, et al. Use of Morphometric Mapping to Characterise Symptomatic Chiari-Like Malformation, Secondary Syringomyelia and Associated Brachycephaly in the Cavalier King Charles Spaniel. PloS one 2017;12(1):e0170315.
35. Stockard C, H. The Genetic and Endondocrinic Basis for Differences in Form and Behavior. Philadelphia: The Wistar Institute of anatomy and Biology; 1941.
36. Marchant TW, Johnson EJ, McTeir L, Johnson CI, Gow A, Liuti T, et al. Canine Brachycephaly Is Associated with a Retrotransposon-Mediated Missplicing of SMOC2. Curr Biol 2017;27(11):1573-1584.
37. Choudhri AF. Skull and Scalp. In: Pediatric neuroradiology: Clinical Practice Essentials. New York: Thieme;2017.p. 126-134.
38. Leeuwen KV. Lacunar skull of the newborn infant. The Journal of Pediatrics 1946 /02/01;28(2):193-199.
39. Agrawal D, Steinbok P, Cochrane DD. Significance of beaten copper appearance on skull radiographs in children with isolated sagittal synostosis. Childs Nerv Syst 2007;23(12):1467-1470.
40. Poonia A, Giridhara P, Sheoran D. Copper Beaten Skull. J Pediatr 2019;206:297-297.
41. Bourekas EC, Lanzieri CF. The calvarium. Semin Ultrasound CT and MR. 1994;15(6):424-453.
42. Rusbridge C, Stringer F, Knowler SP. Clinical Application of Diagnostic Imaging of Chiari-Like Malformation and Syringomyelia. Front Vet Sci. 2018; 5: 280.
43. Schmidt MJ, Ondreka N, Sauerbrey M, Volk HA, Rummel C, Kramer M. Volume reduction of the jugular foramina in Cavalier King Charles Spaniels with syringomyelia. BMC Vet Res.2012; doi:10.1186/1746-6148-8-158
44. Fenn J, Schmidt MJ, Simpson H, Driver CJ, Volk HA. Venous sinus volume in the caudal cranial fossa in Cavalier King Charles spaniels with syringomyelia. Vet J 2013;197(3):896-897.
45. Rekate HL. Pathogenesis of hydrocephalus in achondroplastic dwarfs: a review and presentation of a case followed for 22 years. Childs Nerv Syst 2019;35(8):1295-1301.

46. Robson CD, Mulliken JB, Robertson RL, Proctor MR, Steinberger D, Barnes PD, et al. Prominent basal emissary foramina in syndromic craniosynostosis: correlation with phenotypic and molecular diagnoses. AJNR Am J Neuroradiol 2000;21(9):1707-1717.
47. García-Real I, Kass PH, Sturges BK, Wisner ER. Morphometric analysis of the cranial cavity and caudal cranial fossa in the dog: a computerized tomographic study. Vet Radiol Ultrasound 2004;45(1):38-45.
48. Couturier J, Rault D, Cauzinille L. Chiari-like malformation and syringomyelia in normal cavalier King Charles spaniels: a multiple diagnostic imaging approach. J Small Anim Pract 2008;49(9):438-443.
49. Carrera I, Dennis R, Mellor DJ, Penderis J, Sullivan M. Use of magnetic resonance imaging for morphometric analysis of the caudal cranial fossa in Cavalier King Charles Spaniels. Am J Vet Res 2009;70(3):340-345.
50. Cerda-Gonzalez S, Olby NJ, McCullough S, Pease AP, Broadstone R, Osborne JA. Morphology of the caudal fossa in Cavalier King Charles Spaniels. Vet Radiol Ultrasound 2009;50(1):37-46.
51. Schmidt MJ, Biel M, Klumpp S, Schneider M, Kramer M. Evaluation of the volumes of cranial cavities in Cavalier King Charles Spaniels with Chiari-like malformation and other brachycephalic dogs as measured via computed tomography. Am J Vet Res 2009;70(4):508-512.
52. Driver CJ, Rusbridge C, McGonnell IM, Volk HA. Morphometric assessment of cranial volumes in age-matched Cavalier King Charles spaniels with and without syringomyelia. Vet Rec 2010;167(25):978-979.
53. Schmidt MJ, Amort KH, Failing K, Klingler M, Kramer M, Ondreka N. Comparison of the endocranial- and brain volumes in brachycephalic dogs, mesaticephalic dogs and Cavalier King Charles spaniels in relation to their body weight. Acta Vet Scand 2014;56:30.
54. Sokołowski W, Czubaj N, Skibniewski M, Barszcz K, Kupczyńska M, Kinda W, et al. Rostral cranial fossa as a site for cerebrospinal fluid drainage - volumetric studies in dog breeds of different size and morphotype. BMC Vet Res 2018; doi:10.1186/s12917-018-1483-3
55. Pindrik J, Ye X, Ji BG, Pendleton C, Ahn ES. Anterior fontanelle closure and size in full-term children based on head computed tomography. Clin Pediatr (Phila) 2014;53(12):1149-1157.
56. Hayes AF, Krippendorff K. Answering the Call for a Standard Reliability Measure for Coding Data. Communication Methods and Measures 2007;1(1):77-89.
57. Krippendorff K. Reliability in Content Analysis: Some Common Misconceptions and Recommendations. Human Communication Research 2004;30(3):411-433.
58. Koo TK, Li MY. A Guideline of Selecting and Reporting Intraclass Correlation Coefficients for Reliability Research. J Chiropr Med 2016;15:155-163.

Abbreviations

CI: confidence interval

CM: Chiari-like malformation

CT: computed tomography

ICC: intraclass correlation coefficient

PF: persistent fontanelle

SM: syringomyelia

Declarations

Ethics approval and consent to participate: No human subjects, human material, or human data were involved in this research.

Consent for publication: Not applicable.

Availability of data and materials: Data and materials are available from the corresponding author on reasonable request.

Competing interests: A-M.K. and T.S.J. are part of the Finnish Kennel Club Neurology advisory group.

Funding: The Finnish Veterinary Foundation and Agria/Svenska Kennelklubben Forskningsfond (grant number N2018-0024) supported the study with grants.

Authors' contributions: All authors contributed to the study design. A-M.K. examined all the patients. A-M.K., and T.S.J. analyzed the CT images. J.T.J. performed the statistical analysis. A-M.K. drafted the manuscript with the help of all the co-authors. All authors read,

commented on, and approved the final version of the manuscript.

Acknowledgements: We would like to thank the Finnish Chihuahua Club and Chihuahua owners for their participation in the study and The Finnish Veterinary Foundation, Agria/Svenska Kennelklubben Forskningsfond, and The Veterinary Teaching Hospital of Helsinki University for financial support of the study. Furthermore, we want to thank all the Veterinary Teaching Hospital's radiology technicians for their expertise in providing the CT images.

Tables

Table 1: sutures affected per dog.

Number of affected sutures	Number of dogs	Percentage from all dogs (%)
0	4	8.2
1	21	42.9
2	9	18.4
3	4	8.2
4	3	6.1
5	1	2.0
6	3	6.1
7	2	4.1
8	1	2.0
9	0	0
10	1	2.0
Total	49	100.0

Table 2: Fontanelles affected per dog

Number of fontanelles	Number of dogs	Percentage from all fontanelles (%)
0	4	8.2
1	19	38.8
2	11	22.4
3	2	4.1
4	3	6.1
5	2	4.1
6	2	4.1
7	1	2.0
8	2	4.1
9	0	0
10	1	2.0
11	1	2.0
12	0	0
13	1	2.0
Total	49	100.0

Table 3: Cranial sutures and fontanelles evaluated

Location	Bone	Connecting bone	Suture/intersection	Figure/No:	Human /canine fontanelle equivalent	Number of dogs	Number of sutures	% of all sutures	Number of fontanelles	% of fontanelles
Dorsal sutures	Frontal	Nasal, maxillar, lacrimal	Frontonasal, frontomaxillar, frontolacrimal	Fig 7, No. 1	NA	49	2	1.7	2	1.4
		Frontal	Interfrontal	Fig 7, No. 2	NA	49	4	3.4	4	2.9
		Parietal	Frontoparietal	Fig. 7, No. 3	Bregmatic	49	39	33.1	54	38.8
	Parietal	Parietal	Sagittal	Fig. 7, No. 4	NA	49	0	0	0	0
		Left interparietal	Left parietointerparietal	Fig. 7, No. 5	NA	49	6	5.1	6	4.3
		Right interparietal	Right parietointerparietal	Fig. 7, No. 6	NA	49	6	5.1	6	4.3
Lateral sutures	Frontal	Palatinal, sphenoid	Left frontopalatine, sphenofrontal,	Fig. 8, No. 7	NA	50	1	0.8	1	0.7
			Right frontopalatine, sphenofrontal	NA	NA	50	1	0.8	1	0.7
		Sphenoid, parietal	Left intersection	Fig. 8, No. 8	Left sphenoid	50	3	2.5	3	2.2
			Right intersection	NA	Right sphenoid	50	4	3.4	4	2.9
	Parietal	Sphenoid, temporal	Left sphenoparietal, squamous	Fig. 8, No. 9	NA	50	3	2.5	3	2.2
			Right sphenoparietal, squamous	NA	NA	50	5	4.2	5	3.6
Caudal sutures	Occipital	Parietal	Left occipitoparietal	Fig. 9, No. 10	NA	50	4	3.4	4	2.9
			Right occipitoparietal	Fig. 9, No. 11	NA	50	7	5.9	9	6.5
		Parietal, temporal	Left intersection	Fig. 9, No. 12	Left mastoid	50	12	10.2	13	9.4
			Right intersection	Fig. 9, No. 13	Right mastoid	50	14	11.9	15	10.9
		Temporal	Left occipitosquamous	Fig. 9, No. 14	NA	50	1	0.8	1	0.7
			Right occipitosquamous	Fig. 9, No. 15	NA	50	2	1.7	2	1.4
		Interparietal	Not a true suture	Fig. 9, No. 16	Posterior	50	4	3.4	5	3.6

The sutures are grouped by dorsal, lateral and caudal surfaces, and the bones that the sutures are connecting are nominated. In case the sutural intersections form a fontanelle, the veterinary or a human equivalent term is given. Additionally, the figure in which the suture is visualized and the number marking it is provided.

NA: not applicable, Fig.: figure, No.: number

Table 4.

Inter-rater reliability: Repeatability and Krippendorff's alpha reliability estimates between assessors

Area measured	Repeatability (%)	alpha	95% CI	number of pairs
Total fontanelle area	99.8	0.999	0.997-1.000	50
Dorsal fontanelle area	99.6	0.997	0.995-0.999	50
Left lateral fontanelle area	99.7	0.998	0.995-1.000	6
Right lateral fontanelle area	99.5	0.996	0.989-1.000	9
Caudal fontanelle area	99.6	0.997	0.994-0.999	50

Inter-rater reliability: Repeatability and Krippendorff's alpha reliability estimates of total, dorsal, left and right lateral, and caudal fontanelle area measurements between the two assessors. CI: confidence interval.

Table 5.

Intra-rater reliability: fontanelle area intra-class correlation coefficient

	Assessor 1		Assessor 2		Combined	
Area measured	ICC	95% CI	ICC	95% CI	ICC	95% CI
Total fontanelle area	0.999	0.997-0.999	0.997	0.994-0.999	0.998	0.996-0.999
Dorsal fontanelle area	0.999	0.998-1.000	0.998	0.995-0.999	0.999	0.997-0.999
Left lateral fontanelle area	0.996	0.970-1.000	0.999	0.988-1.000	0.997	0.987-0.999
Right lateral fontanelle area	0.999	0.989-1.000	1.000	0.996-1.000	0.999	0.995-1.000
Caudal fontanelle area	0.993	0.984-0.997	0.992	0.981-0.996	0.992	0.986-0.995

Intra-rater reliability: Fontanelle area intra-class correlation coefficient to assess the repeatability of the measurement of the total, dorsal, left and right lateral, and caudal fontanelle area measurements. ICC: intra class coefficient, ICC: intra class correlation coefficient, CI: confidence interval.

Figures

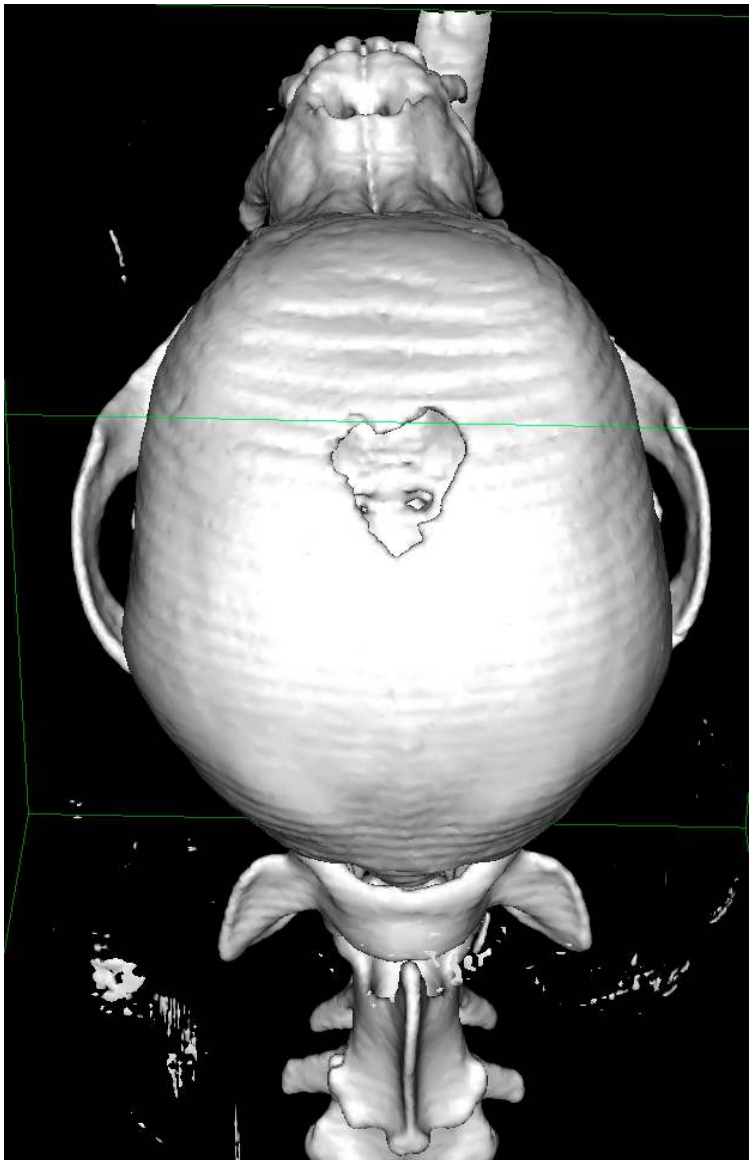

Figure 1

Bregmatic fontanelle. A volume-rendering technique computed tomography image of a Chihuahua skull in dorsal view showing a single, sharply demarcated persistent bregmatic fontanelle at the intersection of the paired frontal and parietal cranial bones (the frontoparietal suture).

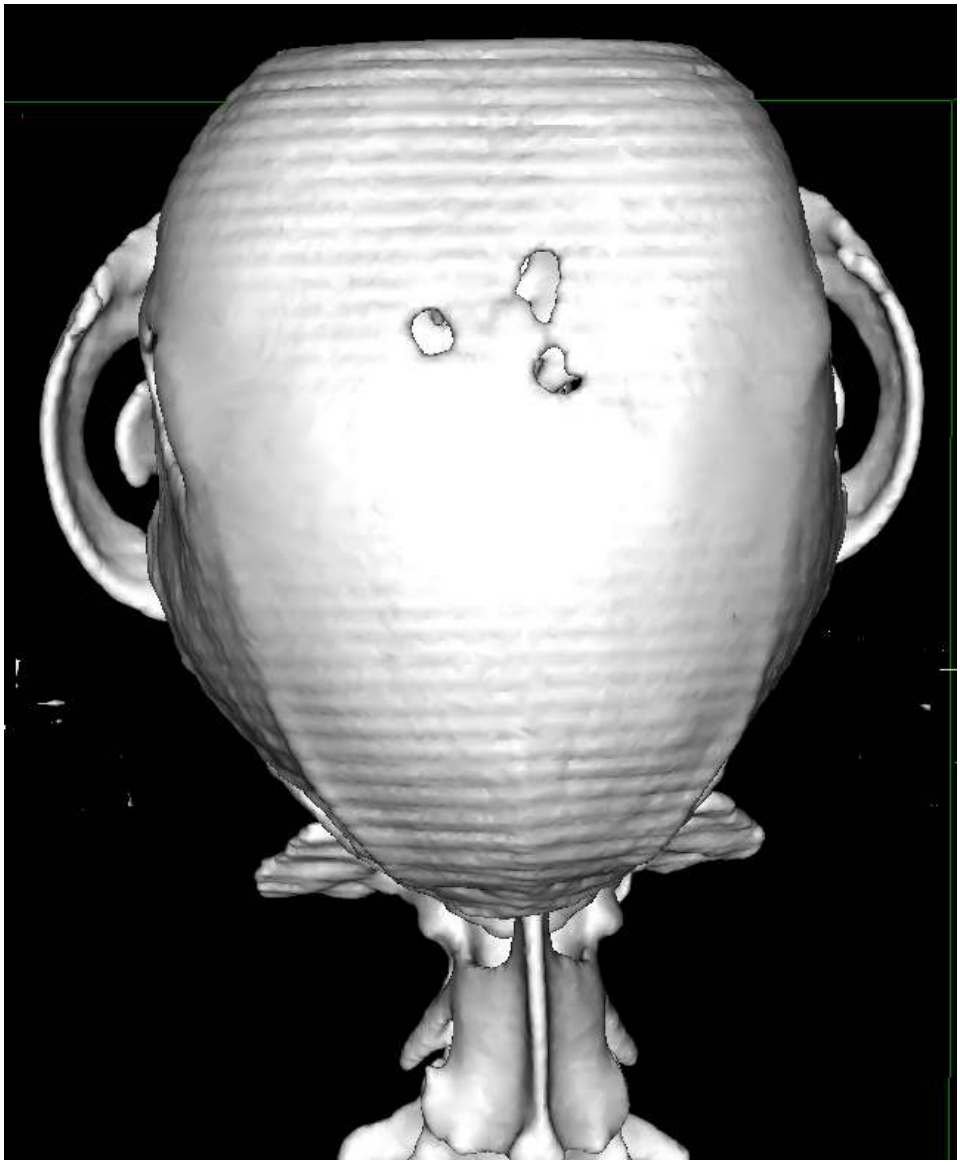

Figure 2

Multiple bregmatic fontanelles. A volume-rendering technique computed tomography image of a Chihuahua skull in dorsal view showing multiple, sharply demarcated persistent bregmatic fontanelles at the intersection of the paired frontal and parietal cranial bones (the frontoparietal suture).

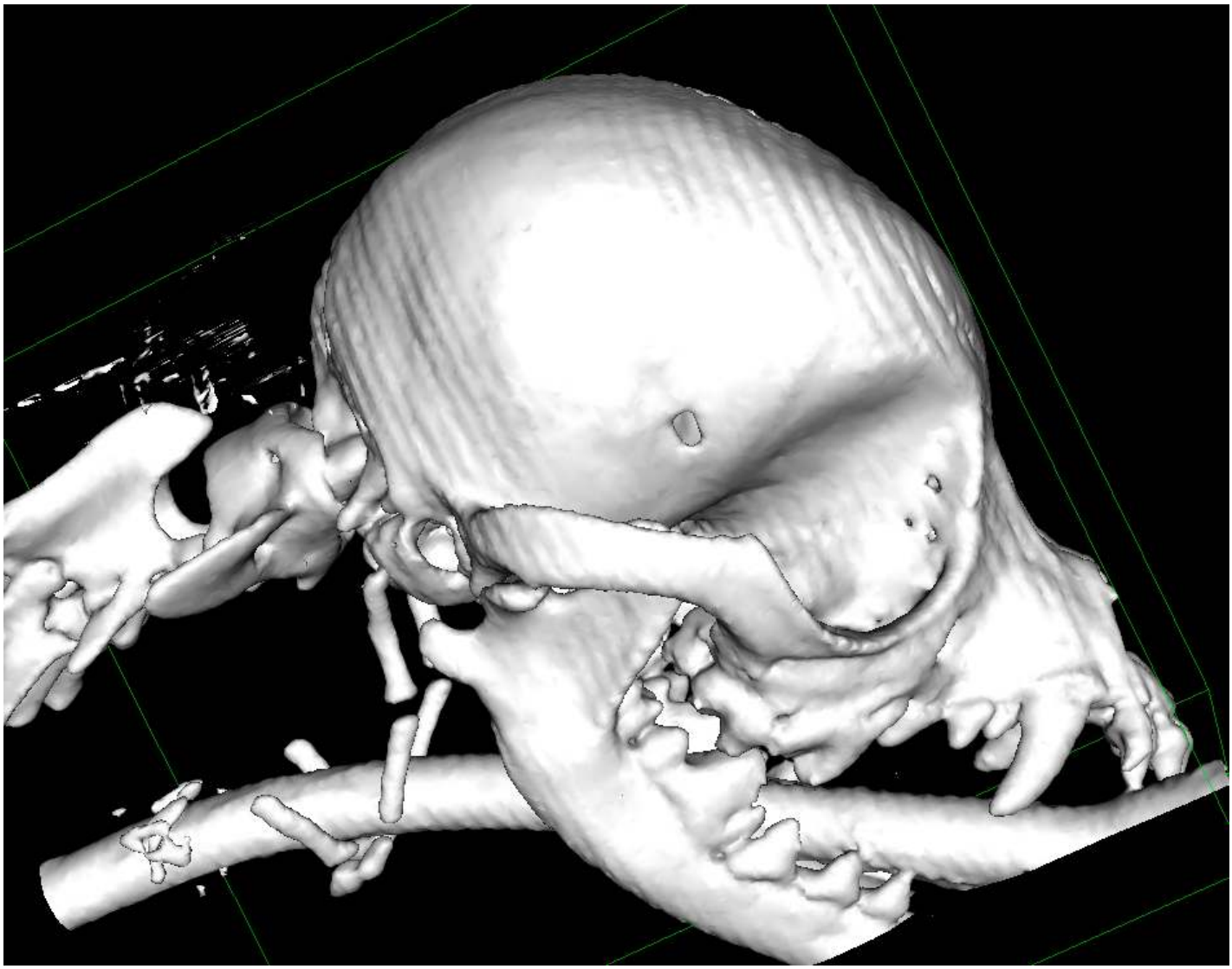

Figure 3

Sphenoidal fontanelle. A volume-rendering technique computed tomography image of a Chihuahua skull in right lateral view showing a single, sharply demarcated persistent fontanelle at the intersection of the frontal, sphenoidal, and parietal bones, resembling the location of the right sphenoidal fontanelle in children.

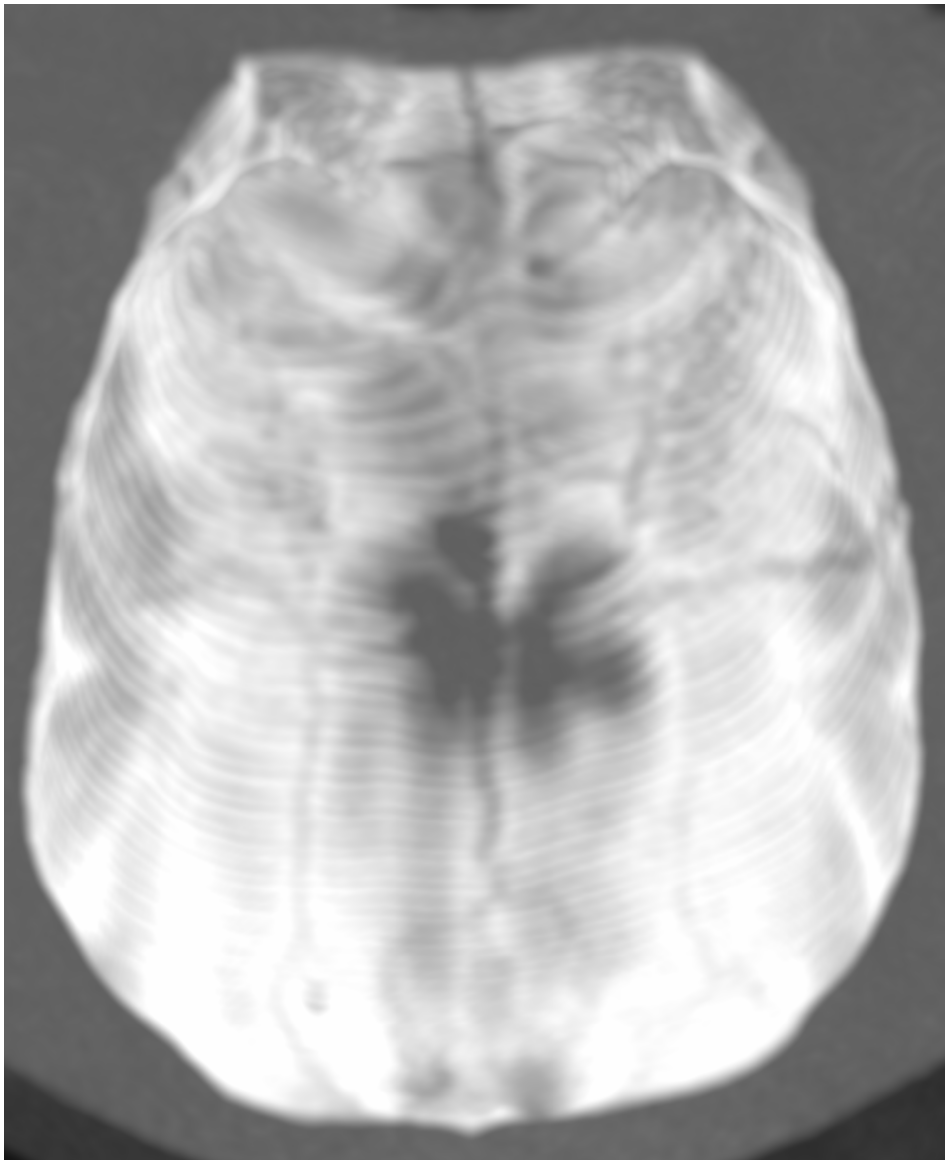

Figure 4

Bregmatic fontanelle with indistinct margins. A dorsal maximum-intensity projection computed tomography image (window level 500, window width 3500, slice thickness 15mm) of a Chihuahua skull with a bregmatic fontanelle with indistinct margins between the paired frontal and parietal bones.

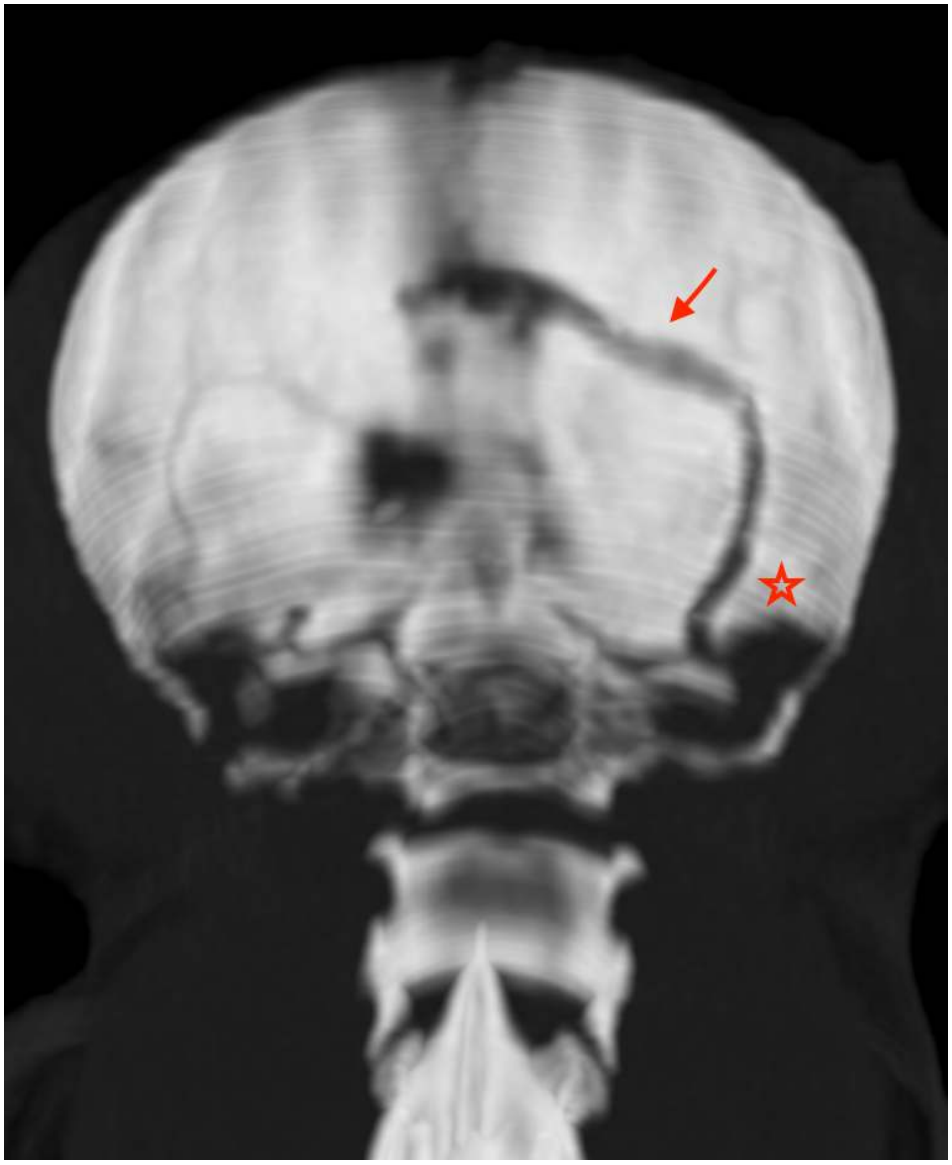

Figure 5

Persistent fontanelle connected to a radiolucent line resembling a venous structure Caudal maximum-intensity projection computed tomography image (window level 500, window width 3500, slice thickness 15mm) of a Chihuahua skull with multiple persistent fontanelles. A persistent fontanelle, located between the right interparietal and parietal bones, is connected to a radiolucent line resembling a venous structure (arrow). The radiolucent line appears to be connected to a persistent fontanelle at the location of the right mastoid fontanelle (star) between the right parietal, occipital, and temporal bones.

Figure 6

Multiple persistent fontanelles on a caudal cranial surface. Volume-rendering technique computed tomography image of a Chihuahua skull in caudal view showing multiple, sharply demarcated persistent fontanelles and an enlarged foramen magnum. The persistent fontanelles (red star) were confirmed in multiplanar images to penetrate through the bone. The rest of the lesions appearing as persistent fontanelles (without a red star) are areas of thin bone.

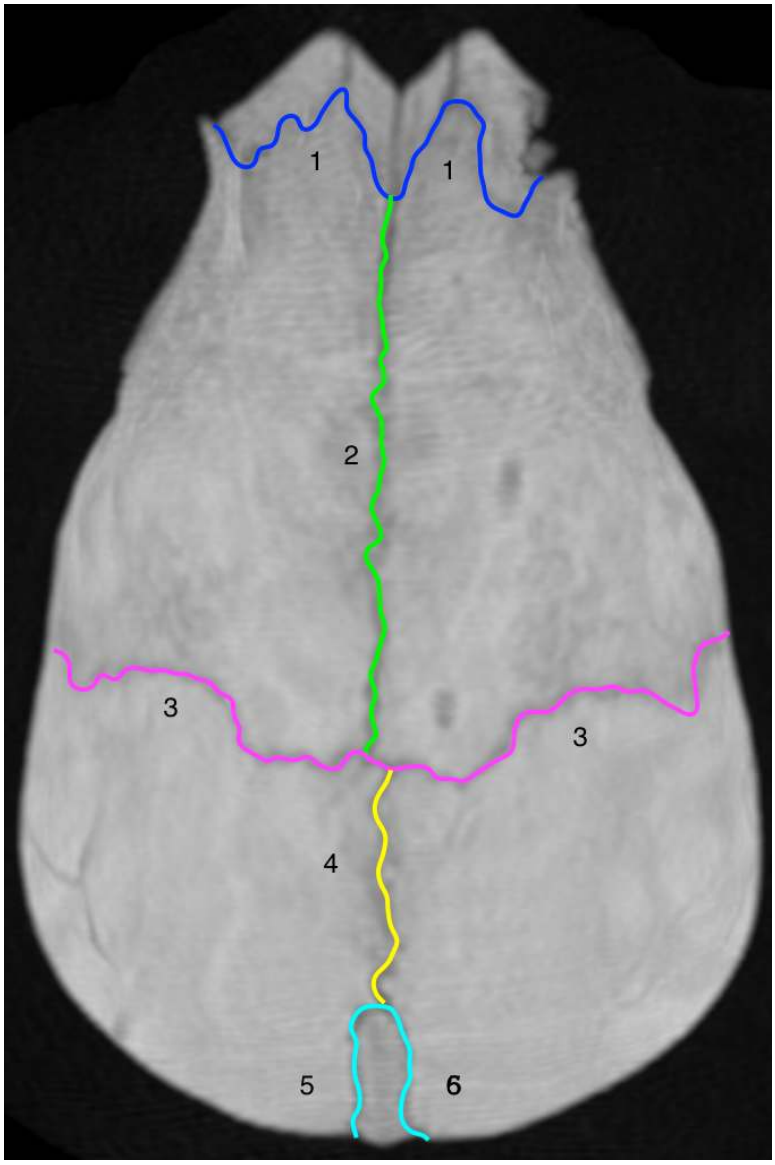

Figure 7

Dorsal cranial sutures Dorsal maximum-intensity projection computed tomography image (window level 500, window width 3500, slice thickness 25mm) of a mixed-breed dog's (weight 5.1 kg) skull: Numbers 1-6 mark dorsal cranial sutures evaluated in the study. (See Table 3 for sutures and connecting bones.) To be able to show the dorsal cranial sutures in one plane, we selected a mixed-breed dog with less doming of the head than in Chihuahuas.

Figure 8

Lateral cranial sutures A left lateral maximum-intensity projection computed tomography image (window level 500, window width 3500, slice thickness 25mm) of a mixed-breed dog's (weight, 5.1 kg) skull: Numbers 3 and 7-9 mark dorsal and lateral cranial sutures evaluated in the study. (See Table 3 for details of sutures and connecting bones.) To be able to show the lateral cranial sutures in one plane, we selected a mixed-breed dog with less doming of the head than in Chihuahuas.

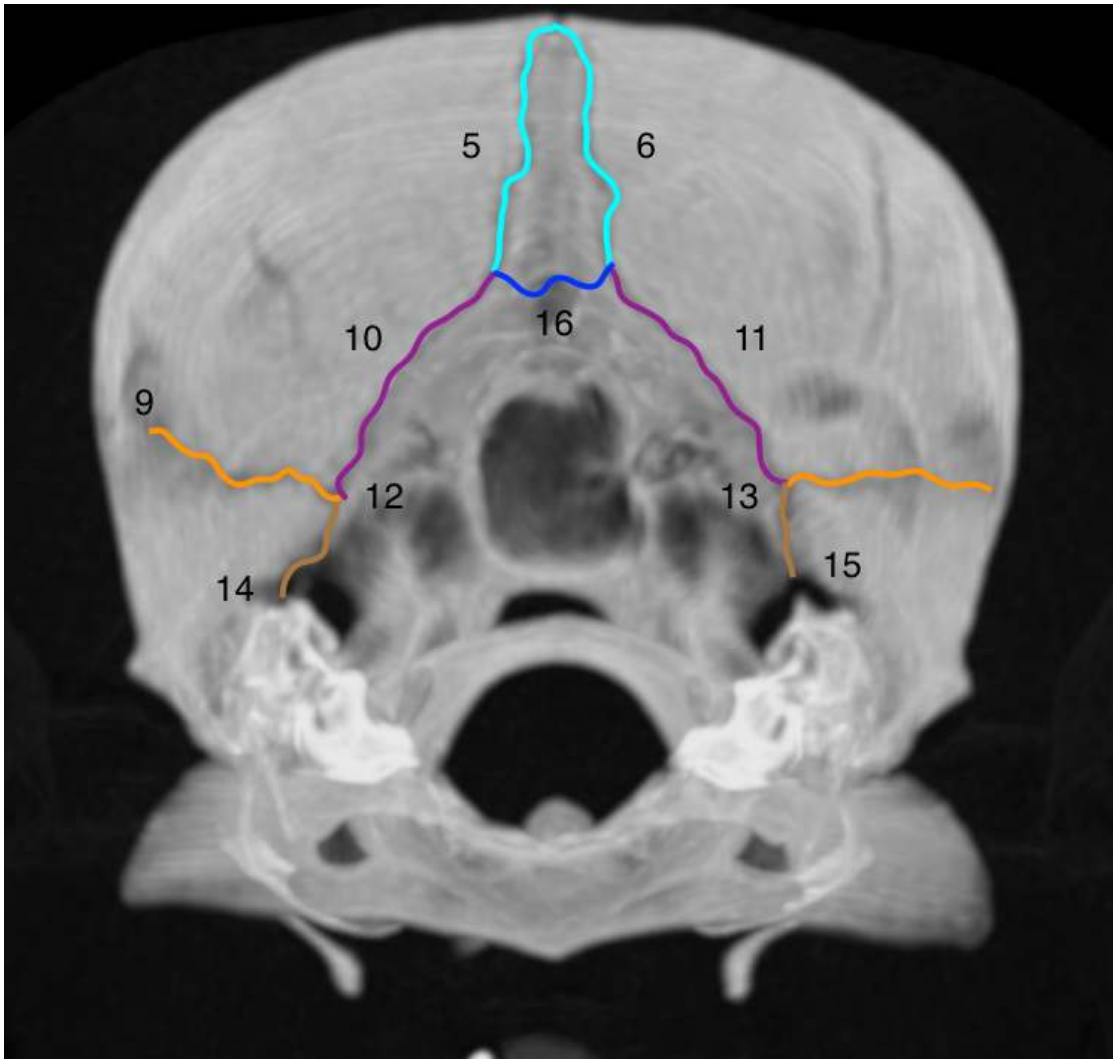

Figure 9

Caudal cranial sutures Caudal maximum-intensity projection computed tomography image (window level 500, window width 3500, slice thickness 25mm) of a mixed-breed dog's (weight, 5.1 kg) skull: Numbers 5-6 and 9-16 mark dorsal, lateral and caudal cranial sutures evaluated in the study. (See Table 3 for details of sutures and connecting bones.) To be able to show the lateral cranial sutures in one plane, we selected a mixed-breed dog with less doming of the head than in Chihuahuas.

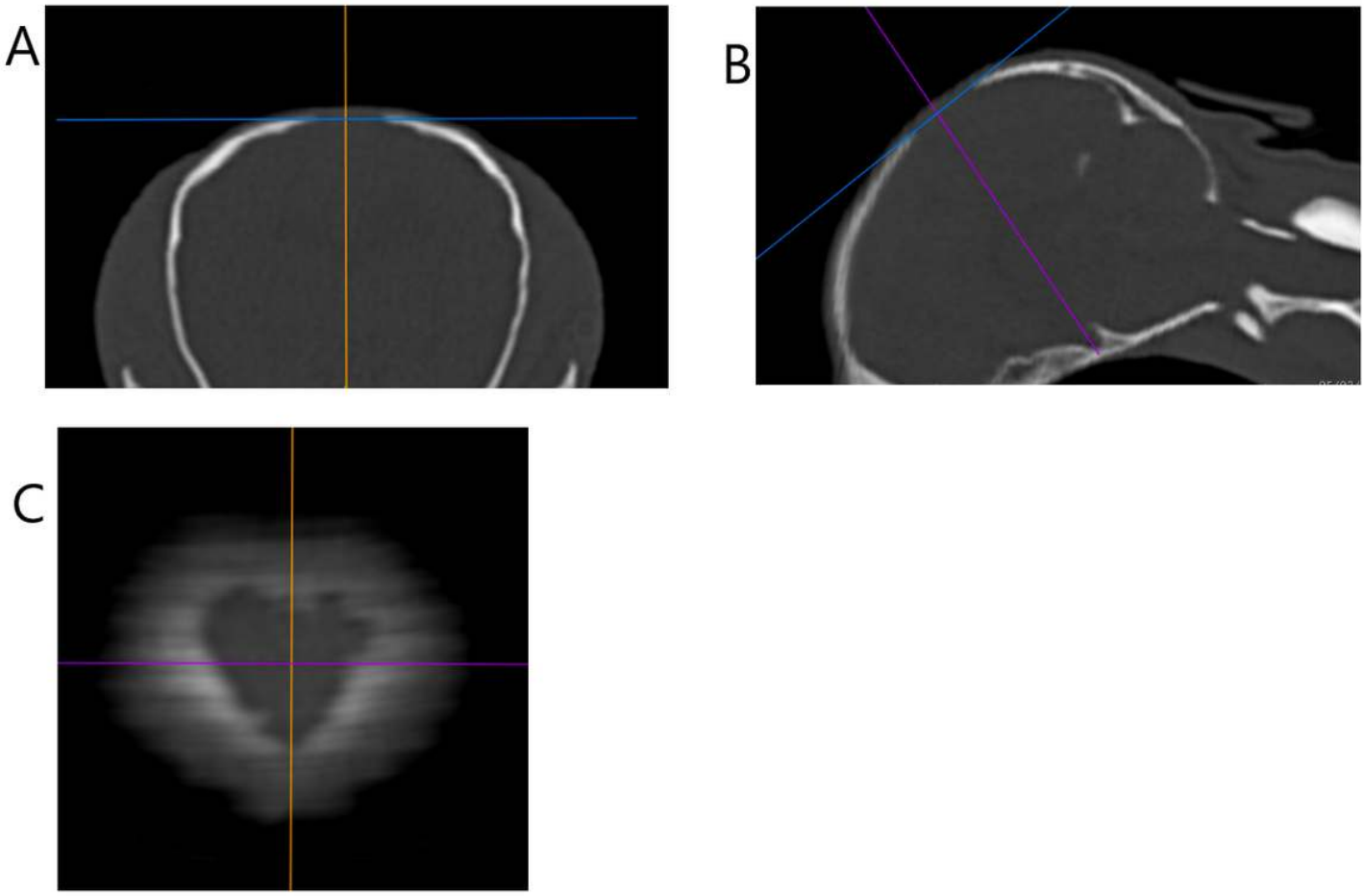

Figure 10

Positioning of the index lines Transverse (a), sagittal (b) and dorsal (c) multiplanar computed tomography images, (window level 500, window width 3500, slice thickness 1 mm) showing the position of index lines positioned so that the first index line was tangential to the outer skull surface and in the mid-thickness of the bone surrounding it (blue index line). The second index line was positioned perpendicular to the previous index line and in the center of the persistent fontanelle (yellow index line in Fig 10a, purple index line in Fig 10b). In the dorsal view (Fig 10c), the intersection of the index lines was positioned at the center of the persistent fontanelle.

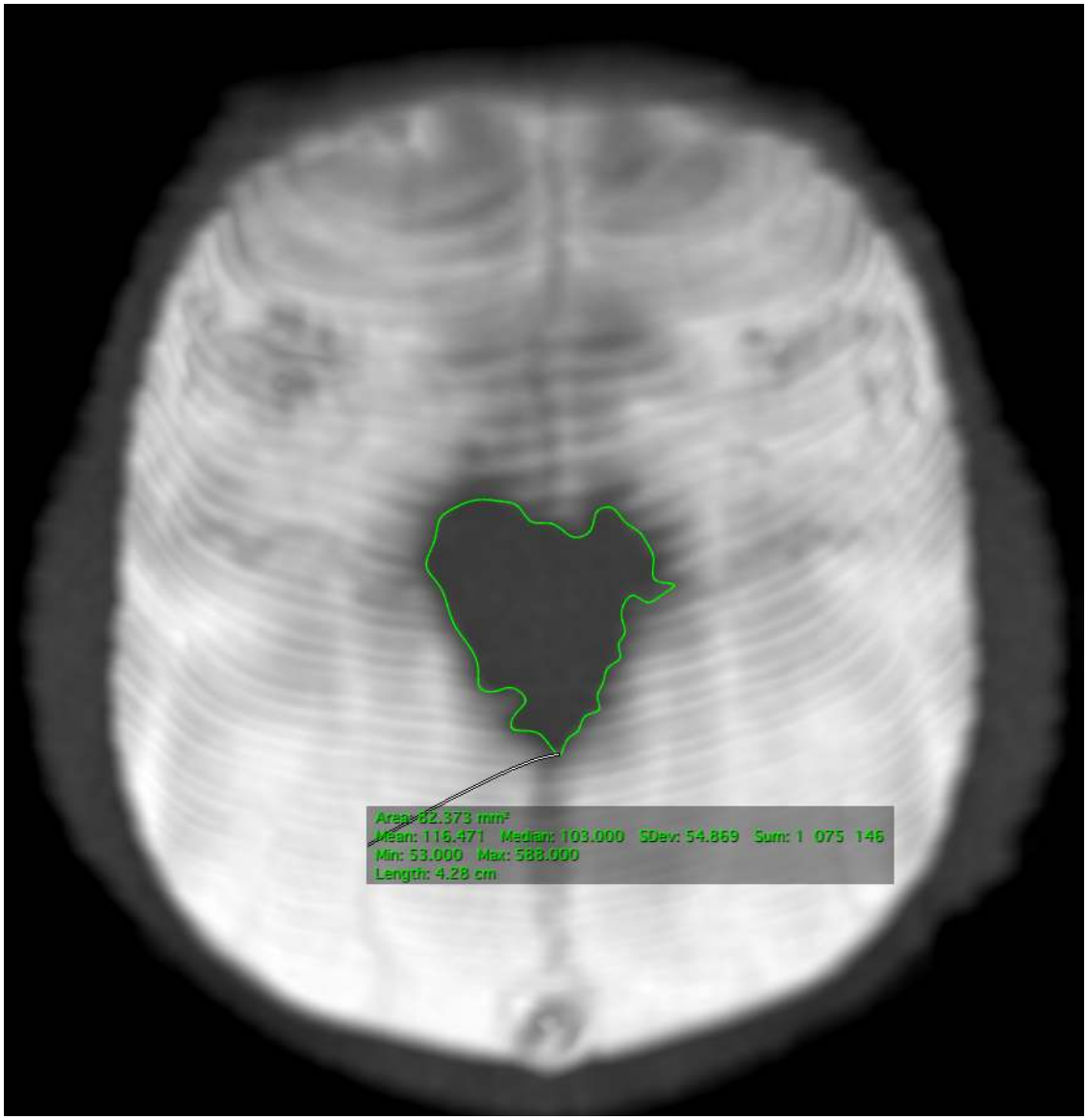

Figure 11

Fontanelle area measurement Dorsal maximum-intensity projection computed tomography image (window level 500, window width 3500, slice thickness 15mm) of a Chihuahua skull with a bregmatic fontanelle between the paired frontal and parietal bones. The area of the bregmatic fontanelle, 82.4 mm2, is measured by OsiriX Medical Imaging Software's closed polygon tool.

Supplementary Files

This is a list of supplementary files associated with this preprint. Click to download.

- KivirantaNC3RsARRIVEGuidelinesChecklist2014.docx